Fundamentals of Multiple-Quantum Magic-Angle Spinning NMR on Half-Integer Quadrupolar Nuclei

Lucio Frydman

Volume 9, pp 262–274

in

Encyclopedia of Nuclear Magnetic Resonance
Volume 9: Advances in NMR
(ISBN 0471 49082 2)

Edited by

David M. Grant and Robin K. Harris

Fundamentals of Multiple-Quantum Magic-Angle Spinning NMR on Half-Integer Quadrupolar Nuclei

Lucio Frydman

Department of Chemical Physics, Weizmann Institute of Sciences, Rehovot, Israel

1	Introduction	1
2	Second Order Quadrupole Effects: Origins and Averaging Approaches	2
3	MQMAS NMR Pulse Sequences	5
4	Fine Structure of the MQMAS NMR Line Shapes	10
5	Outlook	11
6	Related Articles in this Volume	12
7	Related Articles in Volumes 1–8	12
8	References	12

1 INTRODUCTION

A majority of magnetically active nuclides in the Periodic Table possesses half-integer spin numbers: $S = 3/2$, 5/2, 7/2 and 9/2 (Figure 1).[1] Unlike their more common spin-1/2 counterparts, these nuclei possess quadrupole moments and thus interact not only with external or internal magnetic fields, but also with the electric field gradients (EFG) originating from asymmetries in the distribution of charges that surrounds them.[2,3] Depending on the degree of distortion in this local charge distribution, the resulting quadrupole couplings can be small or large when compared to the Zeeman coupling ν_O between the nuclear magnetic moment and the external magnetic field B_o. If sufficiently small, quadrupole effects can often be neglected and the NMR of the spins treated as their $S = 1/2$ counterparts;[4] if comparatively large NMR observations are seldom successful and zero-field nuclear quadrupole resonance (NQR) analyses become the alternative of choice.[3] By contrast to these cases, the majority of scenarios, including those to be considered here, are those where quadrupolar couplings are sizable yet still enable the acquisition of solid state NMR spectra. The resulting quadrupole couplings can then be treated as minor perturbations to a main Zeeman interaction; this leads to broadenings that to first order are orientation-dependent and proportional to the square of the z component of the angular momentum S.[2] For moderately strong quadrupole couplings this implies that when analyzing powdered or disordered samples, all the allowed $\Delta S_z = \pm 1$ transitions will be broadened beyond the NMR detection limit except for the central $-1/2 \leftrightarrow 1/2$ one. It is consequently on these central transitions, which end up being much sharper than the remaining single-quantum signals in the spin manifold, that most solid state NMR studies of half-integer quadrupolar nuclei are generally focused.

In spite of this consideration, central transition quadrupolar NMR spectra do not generally render sharp resonances from powdered samples. This is due to the presence of residual second order quadrupolar broadenings.[2–6] Such higher order effects are proportional to the square of the internal perturbation divided by the main Zeeman interaction, and therefore usually negligible in $S = 1/2$ cases involving shielding or dipolar couplings. They will, however, affect half-integer quadrupoles to an extent proportional to the (quadrupole coupling)$^2/\nu_O$, broadening their central transitions resonances by tens or hundreds of kilohertz whenever EFGs are significant. Analyzing the resulting second order quadrupolar line shapes is not inherently difficult when dealing with individual chemical sites,[4] yet overlap among inequivalent powder patterns precludes these analyses if several inequivalent sites are present. An improvement in the resolution of these solid state line shapes can be achieved by variable-angle sample spinning.[7–9] Yet by contrast to the spin-1/2 case, where first order anisotropies such as the chemical shielding or dipole–dipole interaction can be successfully removed via fast magic angle spinning (MAS), no single 'magic' spinning angle exists capable of removing all the second order effects originated by quadrupolar couplings. This complication stood out as one of the main limitations in the application of solid state quadrupolar NMR, particularly when it came to characterizations of complex materials such as minerals, catalysts, ceramics and glasses.[10]

A better understanding of the nature of second order quadrupole effects has changed this state of affairs. During recent years, a number of different averaging procedures have been proposed, capable of achieving the long-sought goal of bringing high resolution NMR to quadrupolar nuclei.[11–14] All these techniques have in common the introduction of an additional degree of freedom in the manipulation of the spins' evolution; manipulating this extra variable then enables the refocusing of residual second order anisotropies, usually in a two-dimensional (2D) NMR fashion. One approach for implementing such high resolution acquisitions is based on the use of multiple quantum (MQ) spectroscopy in combination with conventional MAS. The resulting technique became known as multiple quantum magic angle spinning (MQMAS),[14,15]

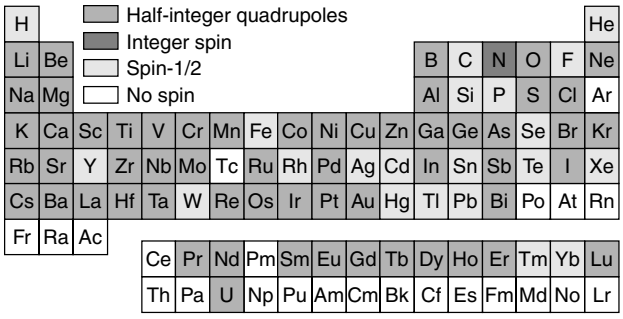

Figure 1 Periodic Table of the Elements indicating the nature of the most abundant NMR-active isotopes. Notice the predominance of half-integer quadrupolar species

and thanks to its ease of implementation it quickly became a method of choice for studies of quadrupolar nuclei in powdered samples. The present article summarizes basic theoretical and practical aspects of MQMAS, as well as limitations to its resolution performance. In its conclusions it also reflects on some of the challenges opened up by the development of this technique.

2 SECOND ORDER QUADRUPOLE EFFECTS: ORIGINS AND AVERAGING APPROACHES

2.1 Second Order Quadrupole Effects

Just as their spin-1/2 counterparts, quadrupolar nuclei possess magnetic moments through which they can interact with magnetic fields. These include the external field B_O, pulsed radiofrequency (rf) fields B_1, local fields generated by the chemical shielding as well as by the dipolar moments of other nuclei. Such magnetic couplings are usually represented by quantum mechanical Hamiltonians: H_Z, H_{RF}, H_{CS}, H_D. In addition, nuclei with $S > 1/2$ are distinguished by a nonspherical shape (Figure 2), associated with a nuclear quadrupole moment capable of coupling with the surrounding electric field gradients. The result is a quantum-mechanical Hamiltonian H_Q that may also end up affecting the NMR transitions. All these local Hamiltonians can be represented by scalar products of spatial and spin tensors of rank $k \leq 2$:[16,17]

$$H_\lambda = C_\lambda \overline{\overline{R}} \cdot \overline{\overline{T}} = C_\lambda \sum_{k=0}^{2} \sum_{m=-k}^{k} (-1)^m R^{(\lambda)}_{k-m} T^{(\lambda)}_{km} e^{-im\omega_0 t} \qquad (1)$$

where $R^{(\lambda)}_{k-m}$, $T^{(\lambda)}_{km}$ define the spatial and spin components of the Hamiltonian, and C_λ is the corresponding coupling constant. Except for $m = 0$ the matrix representation of the T_{km} spin operators is off-diagonal in the usual basis set of Zeeman eigenstates $\{|S_z\rangle\}_{-S \leq S_z \leq S}$. Consequently, analyzing the effects of arbitrary internal Hamiltonians in the presence of the Zeeman coupling is a complex task not always susceptible to analytical treatment. This problem can be simplified when it is possible to assume that all internal interactions H_λ act only as minor perturbations to the main Zeeman coupling. To first order this approximation allows one to consider only those terms that commute with H_Z, which in turn is proportional to T_{10}. Since all internal anisotropies possess rank $k = 2$ this implies that only T_{20} contributions remain. For the quadrupolar Hamiltonian, the resulting first order coupling can be written as

$$H^{(1)}_Q = C_Q R^{(Q)}_{20} T^{(Q)}_{20} = C_Q \sqrt{\frac{1}{6}} R^{(Q)}_{20} [3S_z^2 - S(S+1)] \qquad (2)$$

where $C_Q = \frac{e^2 q Q}{4S(2S-1)h}$ defines the strength of the nuclear quadrupole coupling to the surrounding EFG, and $R^{(Q)}_{20}$ is an irreducible second-rank spherical tensor element depending on the relative orientation between the quadrupole tensor of a given site in a particular crystallite and the Zeeman field. A similar orientation dependence characterizes other first order effects like the dipolar or the chemical shift anisotropies. In principle, all of these anisotropies are susceptible to averaging when executing fast MAS at rates $\nu_r \gg C_\lambda$. Indeed upon mechanical spinning the sample all R^λ_{20} will acquire a time dependence whose average is[3,7,18]

$$\langle R^\lambda_{20}(t) \rangle = R^\lambda_{20} \cdot P_2(\cos\chi) \qquad (3a)$$

where

$$P_2(\cos\chi) = \frac{3\cos^2\chi - 1}{2} \qquad (3b)$$

is the second order Legèndre polynomial possessing a root at $\cos\chi = 1/\sqrt{3}$. Setting the spinning axis at the magic angle $\chi = 54.7°$ with respect to B_O effectively nulls this geometric scaling factor, thereby removing all anisotropic contributions to the solid NMR Hamiltonian.

Achieving such a fast spinning regime in quadrupolar cases is actually difficult in a majority of nuclei by virtue of the large size of their quadrupole moments. Even so, it is possible to avoid the effects of first order quadrupolar anisotropies thanks to the T_{20}-type dependence that characterizes these effects [equation (2)]. The S_z^2 factor in T_{20} then frees the $-1/2 \leftrightarrow +1/2$ transition of first order quadrupolar influences, and is in turn the reason why half-integer quadrupolar studies have generally focused on this central transition.

In spite of this consideration, central transition experiments do not generally afford well resolved resonances. This is due to the large magnitudes of the quadrupolar couplings usually involved, which do not justify the neglect of higher order effects. Particularly important to consider are the second order corrections that the full quadrupolar Hamiltonian will impart onto the spin energy eigenvalues. Standard perturbation theory enables one to represent these effects by[5]

$$H^{(2)}_Q = \frac{C_Q^2}{\nu_O} \sum_{m \neq 0} \frac{R^{(Q)}_{2m} R^{(Q)}_{2-m} [T_{2m}, T_{2-m}]}{2m} \qquad (4a)$$

$$H^{(2)}_Q = -\frac{C_Q^2}{2\nu_O} \left\{ \begin{array}{l} R^{(Q)}_{2-1} R^{(Q)}_{21} S_z [4S(S+1) - 8S_z^2 - 1] \\ + R^{(Q)}_{2-2} R^{(Q)}_{22} S_z [2S(S+1) - 2S_z^2 - 1] \end{array} \right\} \qquad (4b)$$

These correction terms are proportional to the square of the quadrupolar couplings scaled by Zeeman interaction, hence leading to the C_Q^2/ν_O dependence characteristic of second order effects. The multiplication of quadrupolar terms in equation (4) also leads to spatial components that transform as *products* of second-rank spherical tensor elements, as opposed to the simpler R_{20} dependence that characterized all first order

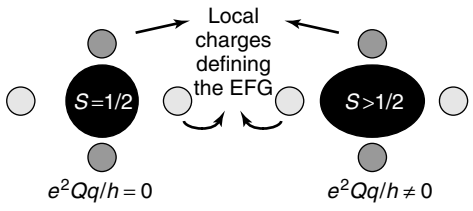

Figure 2 Origin of the electrostatic quadrupole interaction in spins $S \geq 1$, arising from placing the ellipsoidal nuclear positive charge into local electrostatic field gradients. The ensuing coupling ends up depending on the moments of the nucleus, which according to the Wigner–Eckart theorem are in turn proportional to the quantum operators $\{S_\alpha\}_{\alpha=x,y,z}$

effects. Such products result from taking cross correlations of the quadrupolar interaction with itself, and imply that line shapes derived from $H_Q^{(2)}$ will be affected by a net isotropic quadrupolar shift ν_O^Q even though H_Q's original center of mass was zero for all transitions. Also worth mentioning are the products involved in the T_{2m} commutators; these endow $H_Q^{(2)}$ with a spin-space dependence that is different from either T_{10} (linear in S_z) or T_{20} (quadratic in S_z), a feature that will eventually enable MQMAS to refocus second order effects via spin-space manipulations which do not simultaneously remove all chemical shift information.

The presence of isotropic quadrupolar shifts provides a mechanism for distinguishing among chemically inequivalent sites acting in addition to the usual isotropic chemical shift. The anisotropic character of $H_Q^{(2)}$, however, implies that sites in a powder will now also show broad line shapes even when focusing on the central transitions. Furthermore, by contrast to what happened with first order effects, fast MAS of the sample will then be of limited use for assisting in the narrowing of these powder patterns. This is a consequence of the higher complexity associated with the spatial terms of $H_Q^{(2)}$, involving products of second-rank tensors and thus giving origin to both second-(R_{20}) and fourth-rank (R_{40}) anisotropies. The former transform in the usual $P_2(\cos\chi)$ fashion and can thus be removed by MAS; the latter by contrast scale upon sample spinning as the fourth-rank Legèndre polynomial $P_4(\cos\chi) = (35\cos^4\chi - 30\cos^2\chi + 3)/8$, which can be set to zero at some spinning angles but not when $\chi = 54.7°$ (Figure 3). The noncoincident roots of these two polynomials implies that no single choice of spinning axis will simultaneously remove all second order quadrupolar broadenings from a central transition spectrum.[5,11,19]

2.2 Alternatives to Refocus the Anisotropies

One way of remedying this single-axis spinning deficiency is by introducing more complex forms of mechanical reorientation; for instance, by consecutively spinning the sample about two different spinning axes. The two sample spinning angles (χ_1, χ_2) will then be associated with corresponding evolution times (t_1, t_2), bringing in turn the idea and the possibility of refocusing anisotropies via a bidimensional (2D) NMR approach. The choice of spinning angles in these dynamic angle spinning (DAS) experiments demands the simultaneous cancellation, at a given time and for all crystallites in the powder, of both the second- and fourth-rank anisotropies arising from the second order effects. It follows from the considerations above that this can be achieved when setting[11,13]

$$P_2(\cos\chi_1)t_1 = -P_2(\cos\chi_2)t_2$$
$$P_4(\cos\chi_1)t_1 = -P_4(\cos\chi_2)t_2 \qquad (5)$$

conditions which do not affect the normal course of the isotropic evolution. At the conclusion of the total $t_1 + t_2$ evolution time, this choice of spinning angles will lead to the formation of an echo signal encoding a purely isotropic evolution, and by synchronous increases in the duration of (t_1, t_2), this procedure can end up affording a high resolution time-domain signal. This stepwise t_1, t_2 refocusing is different from that occurring in MAS, where anisotropies are being continuously removed. Indeed, in DAS, anisotropies are not removed but show up, after Fourier transformation of the 2D time domain signal, correlated along a sharp ridge for each site in the sample. Therefore unlike MAS, DAS does not bring with its higher resolution an effective increase in signal-to-noise; in fact, signal will be lost by virtue of the need for storing the evolving coherences along B_O while the spinning axis is mechanically reoriented from χ_1 to χ_2.

A refocusing similar to that carried out by DAS but involving a single axis of sample rotation is feasible if the restriction to central transition observations is lifted. Indeed it follows from the arguments given earlier that for any half-integer quadrupole nucleus not only the central but in fact any $S_z = -m \leftrightarrow S_z = +m$ MQ transition will be free from the dominant first order quadrupole broadenings (Figure 4). Yet these transistions will still be affected by second order quadrupole effects, opening up the possibility of compensating the residual broadenings affecting their line shapes with those arising in the central $-1/2 \leftrightarrow +1/2$ transition. To explore such a possibility it is necessary to incorporate the transition order m into the explicit description of the second order NMR frequencies. Under rapid sample spinning conditions this calculation leads to the angle- and order-dependent evolution frequency

$$\nu_Q^{(2)}(m,\chi) = A_0^Q C_0^S(m) + A_2^Q(\varphi,\theta)C_2^S(m)P_2(\cos\chi) + A_4^Q(\varphi,\theta)C_4^S(m)P_4(\cos\chi) \qquad (6)$$

where the $\{A_l^Q\}_{l=0,2,4}$ denote the isotropic, second- and fourth-rank quadrupolar contributions, and the $\{C_l^S(m)\}_{l=2,4}$ are polynomials which depend on the spin S and transition order m involved:

$$C_0^S(m) = 2m[S(S+1) - 3m^2] \qquad (7a)$$
$$C_2^S(m) = 2m[8S(S+1) - 12m^2 - 3] \qquad (7b)$$
$$C_4^S(m) = 2m[18S(S+1) - 34m^2 - 5] \qquad (7c)$$

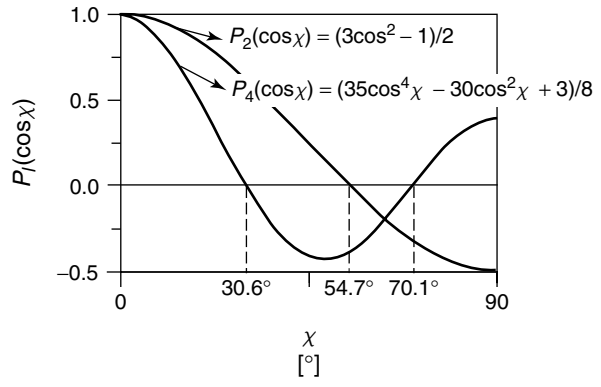

Figure 3 Orientation dependence of the two Legèndre polynomials $\{P_l(\cos\chi)\}_{l=2,4}$ that define the line broadening of central transition quadrupolar patterns. Also shown are the positions of the polynomials' roots: $\chi_m = 54.7°$, the usual magic angle for averaging second-rank anisotropies, and $\chi = 30.6°$, 70.1° for the fourth-rank anisotropies that show up on considering second order effects. The presence of two anisotropic contributions whose zeroes do not coincide deprives sample spinning from the possibility of averaging away central transition broadenings

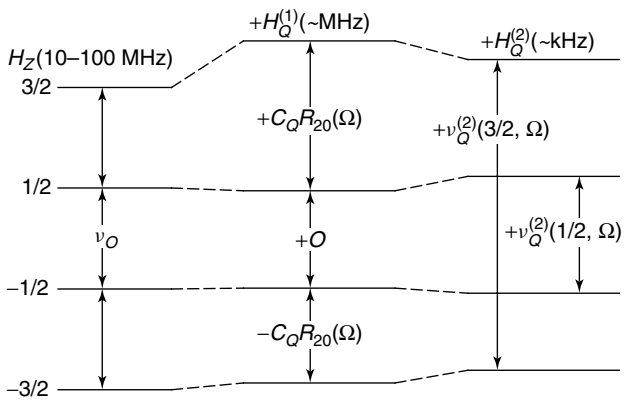

Figure 4 Hierarchical energy level diagram for an $S = 3/2$ nucleus interacting with a dominating external magnetic field coupling and an electric field gradient perturbation

Equation (6) shows the analogous roles that spinning angles and quantum numbers play in defining the second order evolution frequency: the former will scale anisotropies according to the $\{P_l(\cos\chi)\}_{l=2,4}$ polynomials, the latter according to the $\{C_l^S(m)\}_{l=2,4}$ coefficients. Thus instead of fixing m at 1/2 and using χ as a degree of freedom as is done in DAS, it is possible to propose a 2D refocusing experiment whereby for a fixed spinning angle χ spins evolve during initial and final times t_1, t_2 under the effects of two different transition orders m_1 and m_2 (Figure 5). $H_Q^{(2)}$-driven anisotropies will then dephase both of these coherence orders along their respective evolution times, but since these anisotropies can be made proportional to one another for every crystallite the result of such 2D correlation will be powder line shapes that show up as sharp parallel ridges for different sites in the sample.

In analogy to equation (5), the spectral correlation of anisotropic broadenings that is introduced by this MQ strategy can be associated with the time-domain refocusing conditions

$$C_2^S(m_1)t_1 = C_2^S(m_2)t_2 \tag{8a}$$

$$C_4^S(m_1)t_1 = C_4^S(m_2)t_2 \tag{8b}$$

At this (t_1, t_2) point in the MQ correlation, a purely isotropic signal can be detected, which if Fourier transformed would lead to a 1D high resolution NMR spectrum. Although a range of spinning angles χ are compatible with equations (8a,b), the most convenient choice is naturally $\chi_{MAS} = 54.7°$, since under these conditions the hitherto neglected chemical shift and dipolar anisotropies will also be effectively averaged away by the spinning. Simultaneously, MAS makes the second-rank refocusing condition (equation (8a)) immaterial. The selection rules for NMR also need to be considered at this point; these state that in the directly detected domain only single quantum coherences can yield measurable signals, restricting the coherence order to be employed during t_2 to $m_2 = 1/2$; the central single quantum transition. As for the choice of m_1 this may in principle be dictated by the spin number (for $S = 3/2$ only $m_1 = 3/2$ is available; for $S = 5/2 m_1 \leq 5/2$, etc.); yet in all cases at least one such MQ transition is available, and it is the indirect domain that will encode its evolution. Standard phase cycling procedures

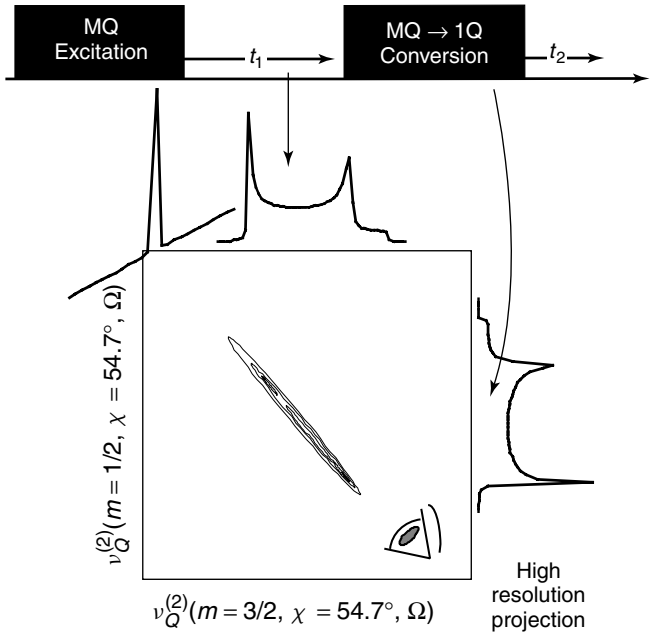

Figure 5 (Top) Schematic diagram of the MQMAS pulse sequence. (Bottom) 2D diagram illustrating how the proportionality among second order MAS broadenings in both the central and MQ transitions, enables high resolution acquisitions when data are considered at appropriate angles in the $MQ \rightarrow 1Q$ 2D correlation spectrum

also put under the experimentalist's control the apparent sense of evolution of the spins during t_1;[20] enabling the stepwise refocusing of all fourth-rank anisotropies regardless of the relative sign of the $C_4^S(m_1)$, $C_4^S(1/2)$ coefficients. As a result of all these considerations, it follows that in MQMAS, second order anisotropies will refocus for all crystallites in the sample simultaneously, at times fulfilling the condition

$$t_2 = \left\{ \frac{|C_4^S(m_1)|}{C_4^S(1/2)} \right\} t_1 \tag{9}$$

The appearance of such long-lived echoes at these particular (t_1, t_2) combinations is one of the most basic features displayed by MQMAS experiments. Their formation is illustrated in Figure 6 for a variety of S and m_1 cases, using ^{23}Na (spin-3/2) and ^{55}Mn (spin-5/2) MQMAS NMR as examples. Rapidly decaying anisotropic evolutions are evident here along both the MQ and 1Q (t_1 and t_2) domains, yet as predicted by equation (9), a much slower decay is noticed along the ideal $|C_4^S(m_1)|/C_4^S(1/2)$ slope.

The capacity of MQMAS NMR to resolve chemically inequivalent sites is further illustrated in Figure 7(a), which shows how this experiment can distinguish four inequivalent ^{23}Na sites that overlap in the conventional MAS spectrum of the Na_2ATP complex. As in the DAS case, it may be convenient to transform the tilted powder patterns that result from these MQMAS experiments into a format that can yield a 1D high resolution trace by conventional projection. This can be done by a shearing transformation defined by the $|C_4^S(m_1)|/C_4^S(1/2)$ ratio; which is in essence a rotation of the line shapes, and can be carried out in such a way as to leave a conventional MAS pattern along one of the spectral axes

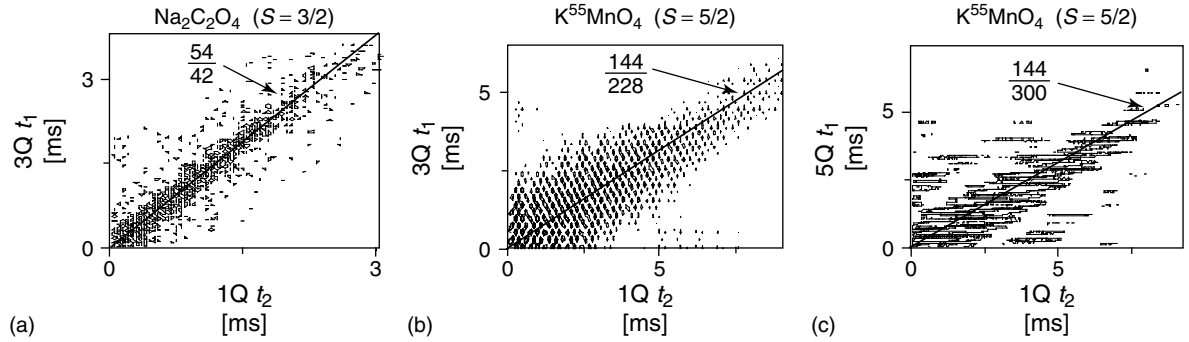

Figure 6 ^{23}Na ($S = 3/2$) and ^{55}Mn ($S = 5/2$) MQMAS NMR time-domain data illustrating the formation of long-lived isotropic echoes at the theoretically expected slopes. (a, b) Triple- to single-quantum correlation experiments; (c) five- to single-quantum correlation experiment

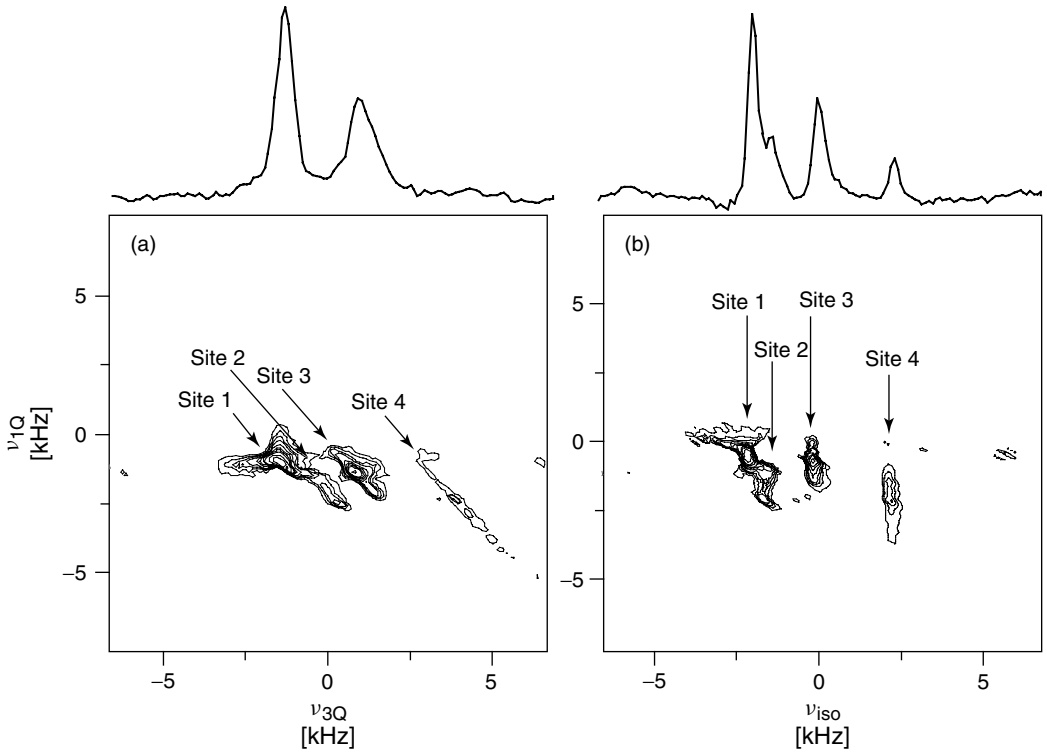

Figure 7 2D 7.1 T ^{23}Na NMR spectrum arising from the $Na_2ATP{\cdot}10H_2O$ complex crystallized from water/dioxane after (a) standard FFT of the 3QMAS time-domain data; (b) subjecting the 2D MQMAS data to a shearing transformation. In both cases the 1Q domain contains the conventional MAS line shapes, distorted by the relative powder efficiencies of the MQ excitation and conversion processes. Sites in (a) appear resolved when regarded at a slope depending on the $|C_4(3/2)/C_4(1/2)|$ ratio; in (b) by contrast, a projection along the indirect domain leads to a purely isotropic high resolution 1D dimension showing four partially resolved resonances (adapted from Ref.[74])

and only isotropic components along the other (Figure 7b). An alternative procedure involves redefining the first evolution period so as to contain all the MQ evolution plus the fraction of 1Q evolution needed for a complete refocusing of anisotropies; such a redefined t_1 time will thus encode a purely isotropic evolution.[21] Pros and cons involved in these and other MQMAS procedures are described in greater detail in the article by Pruski and Amoureux (see **Advances in MQMAS NMR**). Also worth noting is a recently proposed alternative whereby second order effects of the central 1Q transition are refocused not by symmetric MQ transitions, but by their single-quantum counterparts in the satellite transitions[22] (see **Satellite Transition NMR Spectroscopy of Half-Integer Quadrupolar Nuclei under Magic-Angle Spinning**).

3 MQMAS NMR PULSE SEQUENCES

3.1 General Considerations

The previous section introduced some of the problems associated with the acquisition of high resolution NMR spectra in the presence of second order effects, and the manner by which MQMAS enables the removal of the anisotropies via the

stepwise refocusing of MQ dephasings by 1Q spin evolutions. Two active steps are required for the generation of the ensuing MQMAS echoes: a first one involving the excitation of the MQ coherence starting from an equilibrium state, $S_z \rightarrow S_{x,y}^{MQ}$, and a second one involving the conversion of MQ coherences that evolved during t_1 into 1Q coherences whose signals can be detected: $S_{x,y}^{MQ} \rightarrow S_{x,y}^{1Q}$. Several pulse sequences have already been proposed to implement these two steps while undergoing MAS,[14,15,21,23–48] and it is likely that new and better protocols to achieve these goals will continue to arise in the near future. Therefore in an effort to avoid premature obsolescence, this section focuses on general considerations of what such pulse sequences incorporate rather than on their comprehensive individual descriptions.

Before going into specifics, it is worth dwelling on generalities about what a good MQMAS pulse sequence should achieve. As manipulations of MQ coherences by means of rf fields are to first order forbidden by the conventional NMR transition rules, the excitation of MQ coherences and their subsequent transformation into 1Q observables is rarely a very efficient process. Hence if summarizing the initial excitation of MQ coherences according to

$$S_z \xrightarrow[\text{excitation}]{} e_x S_x^{MQ} + e_y S_y^{MQ} \tag{10a}$$

and the subsequent conversion process by

$$\begin{aligned} S_x^{MQ} &\xrightarrow[\text{conversion}]{} c_{xx} S_x^{1Q} + c_{xy} S_y^{1Q} \\ S_y^{MQ} &\xrightarrow[\text{conversion}]{} c_{yx} S_x^{1Q} + c_{yy} S_y^{1Q} \end{aligned} \tag{10b}$$

one of the main goals usually being sought in MQMAS is simply the maximization of the excitation $\{e_i\}_{i=x,y}$ and the conversion $\{c_{ij}\}_{i,j=x,y}$ coefficients. Furthermore the free spin evolutions occurring during t_1 and t_2 are unitary processes involving relatively long spin–spin relaxation decays which preserve the norm of the spin coherences; it is then convenient to introduce a description of the MQMAS signal intensity in terms of a single complex number $\varepsilon = (\varepsilon_x, \varepsilon_y)$ given by[42]

$$\begin{aligned} \varepsilon_x &= [e_x(c_{xx} + c_{yy}) + e_y(c_{yx} - c_{xy})]; \\ \varepsilon_y &= [e_x(c_{xy} + c_{yx}) + e_y(c_{xx} - c_{yy})] \end{aligned} \tag{11}$$

The MQ processes in equations (10a,b) are usually mediated by the simultaneous action of the rf plus the orientation dependent first order quadrupole interaction, and therefore all coefficients in equation (11) will vary from crystallite to crystallite. In view of this, it becomes meaningful to associate an efficient MQMAS sequence with the largest powder averaged value of $|\varepsilon|^2$

$$|\varepsilon|^2 \approx \left\{ \left[\int_{\text{powder}} d\Omega \varepsilon_x(\Omega) \right]^2 + \left[\int_{\text{powder}} d\Omega \varepsilon_y(\Omega) \right]^2 \right\} \tag{12}$$

Yet it also follows from this analysis that there is more to an optimum pulse sequence than achieving the largest possible $|\varepsilon|^2$ value. This stems from the echo character of the MQMAS experiment, which requires all spins to evolve solely from the second order effects active during t_1 and t_2. Conspiring against this requirement is the fact that both the rf-driven excitation and conversion of MQ coherences are orientation dependent processes, a feature which opens up the possibility of imparting extra evolution phases to the spin coherences that do not relate to the second order effects, and hence may fail to refocus during the course of the experiment (Figure 8). For instance a sequence which efficiently transforms S_x^{MQ} into S_x^{1Q} but which at the same time generates an appreciable S_y^{1Q} component may be associated with a large $|\varepsilon|^2$ value, but will at the same time induce a net rotation in the $\{S_x^{1Q}, S_y^{1Q}\}$ space that prevents the full refocusing of anisotropies via the $MQ \rightarrow 1Q$ correlation. It is possible to associate the overall anisotropy of the excitation and conversion processes with the powder distribution of the ε phase factor: $\phi(\Omega) = arctan[\varepsilon_y(\Omega)/\varepsilon_x(\Omega)]$. This parameter describes the relative phase with which the rf pulse sequence itself (as opposed to the actual internal spin interactions) transforms the equilibrium magnetization into observable x and y components via an intermediate MQ step. A narrow distribution of the $\phi(\Omega)$ values over the powdered sample is therefore another important goal to achieve for maximizing the sensitivity. It is also possible to decompose the various x and y pulse sequence coefficients into spherical coordinates and re-express this whole treatment in terms of $\{S_\alpha^{1Q}, S_\alpha^{MQ}\}_{\alpha=\pm}$ spin coherences. One would then state that an important characteristic of any given pulse sequence is not only the absolute efficiencies of its various processes, but also the relative efficiency with which it transforms the $S_z = 0$ magnetization first into separate $+m$ and $-m$ coherences, and subsequently each of these into observable magnetization of coherence order -1. Considerations on the line shape distortions that may then arise in connection with the different efficiencies of the $0 \rightarrow \pm m \rightarrow -1$ coherence transfer pathways are further discussed below, as well as elsewhere (see **Advances in MQMAS NMR**).

3.2 Overview of MQMAS Pulse Sequences

As mentioned, the main actors in the MQMAS pulse sequence excitation and conversion processes are the rf and the first order quadrupole interactions. The former creates the various nonequilibrium states while the latter, even though absent during the evolution and acquisition periods, is in fact the coupling that enables the generation of MQ states. There are also other factors affecting the various stages of the pulse sequence including the spinning speed, which controls the temporal oscillations of the quadrupole coupling during the course of the rf pulses, as well as the shifts arising from the chemical shielding and second order quadrupolar interactions. Additional variables available in the design of the pulse sequences include the amplitudes, phases and frequencies of the various rf pulses involved in the MQ excitation and conversion, as well as the number of pulses involved in each stage. Figure 9 presents a number of strategies that have hitherto been proposed for the implementation the excitation and conversion steps of MQMAS acquisitions on spin-3/2.

Although simple, a sequence composed by two short pulses (Figure 9a) is capable of affording MQMAS spectra and provides insight into the general spin physics of more complex procedures. This experiment involves a short initial pulse which transforms the initial equilibrium polarization into high order MQ coherences, a free evolution period t_1, and a second short pulse that converts the evolving MQ coherences into observable 1Q magnetization. Such pulse sequence was

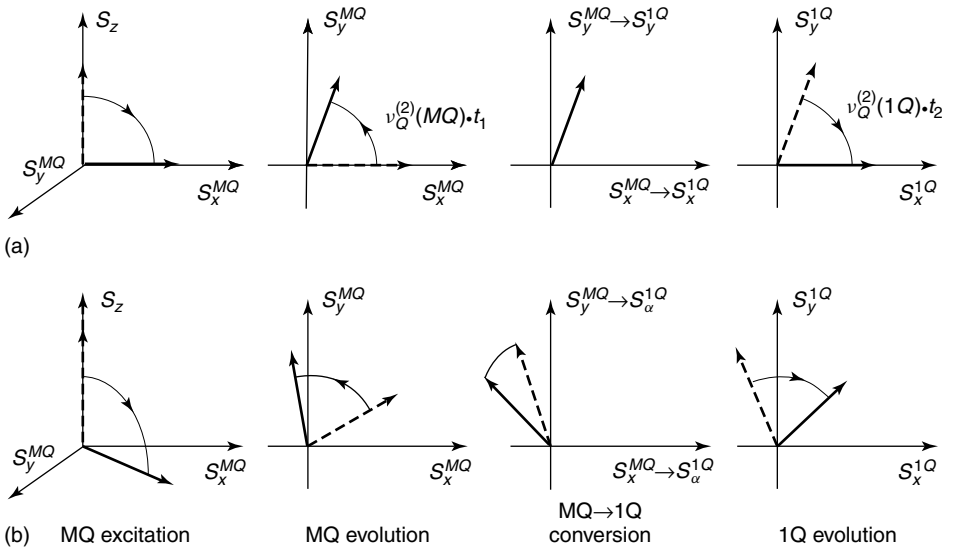

Figure 8 Potential echo spoiling effects of pulses throughout an MQMAS sequence. Dashed lines correspond to the starting spin states, full lines illustrate the finishing states. In an ideal pulse sequence (a) the spin packets of different crystallites evolve under the effects of internal anisotropies and pulses are only responsible for the direct excitation and transfer of coherences among the subspaces. A complete reversal of the anisotropic evolution occurs, and hence magnetizations of all crystallites refocus along a common axis (assumed here to be the x-axis). In actual experiments (b) the orientation dependence of the excitation and conversion processes may induce net evolution phases which prevent a full reversal of anisotropies

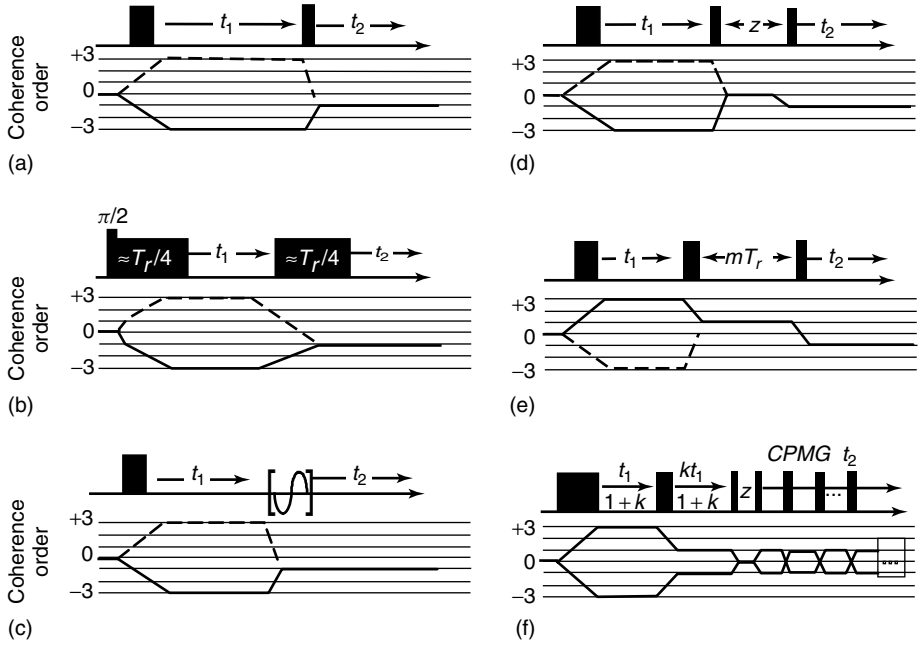

Figure 9 Some of the pulse sequences proposed for the acquisition of 2D MQMAS spectra. (a) Basic two-pulse sequence implementing the excitation and conversion of the multiple-quantum coherences with short CW pulses. (b) Variant based on MQ coherence manipulations driven by adiabatic passages between $MQ \leftrightarrow 1Q$ states, with the initial MQ excitation being aided by a central transition 90 °excitation pulse. (c) Sequence incorporating a fast-amplitude modulation (FAM) of the MQ conversion pulse. In general short CW, RIACT and FAM pulses (as well as other rf pulse modules, such as composite pulses or double-frequency-sweep pulses) can be combined in various forms to achieve a maximization of the MQMAS signal and optimization of the line shapes. Alternatives to the simple MQ(t_1)−1Q(t_2) scheme are shown on the right-hand column and include the introduction of a z-filter (d), whole echo detection during t_2 (e), and a split-t_1 scheme followed by a z-filter and Carr−Purcell−Meiboom−Gill acquisition. Staffs underneath each pulse sequence describe the corresponding coherence transfer pathways required for detecting the MQMAS echo and anti-echo signals (full and dashed lines, respectively). The actual coherence transfer pathway executed during the pulse sequence can be selected either by phase cycling[20,75] or via the application of pulsed field gradients[76]

initially proposed for performing double- and triple-quantum NMR spectroscopy on static powders and single crystals,[49–51] and currently finds widest application in MQMAS experiments on half-integer quadrupolar nuclei. An exact analysis on the nature of this sequence requires propagating the evolution of the spins as a function of all the coupling parameters mentioned earlier (spin number S, transition order m, quadrupole coupling parameters C_Q, η_Q, shielding parameters $\nu_{\text{iso}}^{\text{CS}}$, $\nu_{\text{aniso}}^{\text{CS}}$, Larmor frequency ν_O, spinning rate ν_r, transverse rf nutation field ν_1). Such calculations have been carried out for a range of conditions;[23,28,34,40] they are useful and eventually even necessary, yet sometimes some basic features of the experiment can also be gathered from simpler analytical treatments. One such analysis assumes only static first order quadrupolar and rf Hamiltonians:[15]

$$H_{\text{irr}} = C_Q\sqrt{\frac{1}{6}}R_{20}(\theta,\varphi)[3S_z^2 - S(S+1)] + \nu_1 S_x \qquad (13)$$

Nuclear spins initially in a thermodynamic equilibrium state parallel to the z-axis will be excited by this irradiation to yield, among other states, the desired 3Q coherences. The origins of this MQ excitation process can be appreciated by diagonalizing H_{irr}, and describing the resulting Hamiltonian in terms of fictitious spin-1/2 operators.[51,52] It can then be shown that for a spin $S = 3/2$ the result contains, among other components, a triple-quantum transverse excitation term proportional to S_x^{1-4}. This MQ excitation operator comes as a higher order rf effect mediated by the quadrupolar term, which excites the initial population into S_y^{1-4} coherences according to

$$S_z \xrightarrow{H_{\text{irr}}\tau_{\text{exc}}} 3\sin\left(\frac{3}{8}\frac{\nu_1^3}{\nu_Q^2(\theta,\varphi)}\tau_{\text{exc}}\right)S_y^{1-4} \qquad (14)$$

Note the unusual dependence of the nutation rate, as well as a factor of three magnifying the MQ coherence. The former derives from the higher order nature of this excitation, which scales the effective rf by a factor $(\nu_1/\nu_Q)^2$. The latter derives from the direct $S_z^{1-4} \rightarrow S_y^{1-4}$ process promoted by the S_x^{1-4} excitation term in H_{irr}. Although this prediction of a single nutation frequency for the buildup of single-crystallite triple-quantum coherences is just an approximation, it is quite a good one, mainly if the rf pulse is short enough to neglect other factors such as sample rotation, second order effects, and isotropic/anisotropic offsets. The nutation curves for a powdered sample can then be computed as a weighted superposition of single crystal nutation patterns for all possible (φ, θ); angles (Figure 10a). These theoretical predictions match well with MQMAS NMR experiments and predict that over a range of ν_1/ν_Q ratios, a growth in the MQ excitation occurs for increasing rf fields. This feature has led to the development of customized MQMAS probes capable of delivering intense pulses for short periods of time, reaching in favorable cases nutation rates in excess of 200 kHz. As for more conventional rf settings, one of the main reasons precluding the efficient excitation of MQ coherences with low nutation fields is the relatively long periods required for achieving the desired buildup. These then become comparable to the duration of the rotor period, and the MAS-driven averaging of $H_Q^{(1)}$ deprives the process from much of its effectiveness. Even under such conditions it has been observed

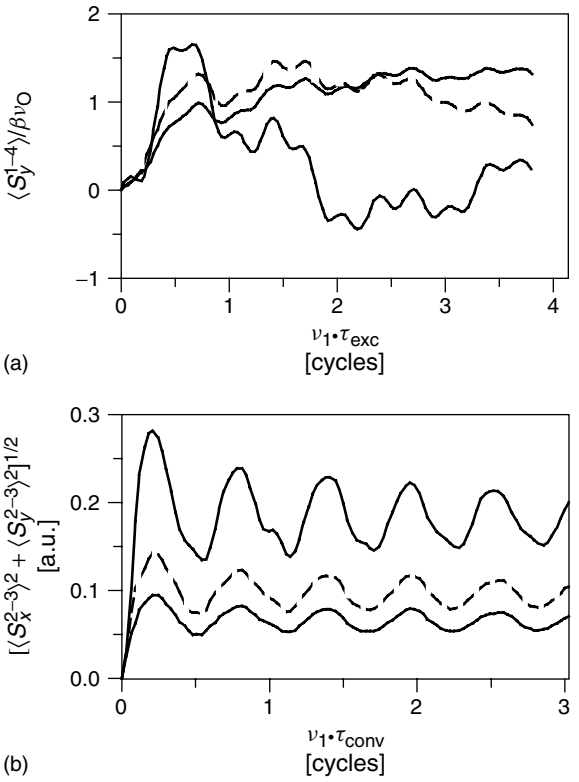

Figure 10 Triple-quantum excitation (a) and conversion (b) nutation behavior expected for a $S = 3/2$ nucleus subject to short CW pulses (sequence in Figure 9a), calculated for a static powdered sample as a function of different C_Q/ν_1 ratios: $C_Q/\nu_1 = 2$ (dotted lines), $C_Q/\nu_1 = 4$ (dashed lines), $C_Q/\nu_1 = 6$ (continuous lines). In all cases an axially symmetric quadrupole tensor with $C_Q = 400$ kHz was assumed; spins were assumed at thermal equilibrium for the excitation calculations, and at $S_x^{1-4} = S_y^{1-4} = 1$ for the $3Q \leftrightarrow 1Q$ conversion ones (adapted from Ref.[15])

that the excitation of MQ coherences can still be carried out continuously through the course of several rotor periods, provided that the amplitudes of the rf nutation fields are set between multiples of the sample spinning speed.[47]

A MQ excitation mechanism approach different from the one just discussed is the rotationally induced adiabatic coherence transfer (RIACT).[26] This effect exploits the fact that MAS will effectively null the quadrupolar frequency of a crystallite a number of times during the course of a rotor period, and that at these zero crossings a transverse rf field may redistribute the spin coherences among all eigenstates within the spin manifold.[53] Coherences that had been initially excited into transverse $\{S_i^{2-3}\}_{i=x,y}$ magnetizations of the central transition may end up during these zero crossings redistributed into higher $\{S_i^{1-4}\}_{i=x,y}$, giving rise to the desired MQ excitation. These experiments will therefore involve an initial central transition pulse, which can usually be made highly efficient for all crystallites in the sample, followed by a spin locking period during which the $1Q \rightarrow MQ$ transfer occurs (Figure 9b). In order to ensure that most crystallites in the sample undergo at least one zero crossing but avoid the occurrence of multiple crossings (which would transfer coherence back from $MQ \rightarrow 1Q$), the RIACT spin-lock excitation is usually kept within 1/4–1/3 of a rotor period.

Under optimal conditions of adiabatic passage, the transfer will be complete for all crystallites regardless of their individual quadrupolar frequencies and thus exhibit an improvement over the short-pulse approach in Figure 9(a).

Both short continuous wave (CW) as well as spin-locking pulses can be used as starting points for implementing the $MQ \rightarrow 1Q$ conversion process. Indeed it can be shown that such conversions involve simultaneous manipulations of the satellite $\pm 1/2 \leftrightarrow \pm 3/2$, amenable to both kinds of pulse sequences. Furthermore, similar theoretical approaches to those used in the excitation can be employed to design sequences that optimize the MQ to single-quantum conversion processes. These show that in the presence of large first and second order quadrupolar effects both strategies are actually challenged; the short CW one by the high rf fields that it requires for meaningful excitations of the satellite transitions, and RIACT by its marked orientation and offset dependencies. For instance, in the short pulse case it can be shown that in contrast to the MQ excitation case [equation (14)], the conversion process possesses no well-defined nutation frequency for the various crystallites. This in turn leads to a relatively poor conversion efficiency even for a single crystal orientation, as well as to one which rapidly decreases with increasing C_Q/ν_1 ratios. Still, even for powder samples, a maximum at $\nu_1/\tau_{\text{conv}} \approx 0.2$ cycles can be localized corresponding to a transient coherent superposition of the individual single crystal signals (Figure 10b).[15,23] Furthermore, rotational resonance excitation conditions for rf nutation rates $\nu_1 \approx \nu_r$, $2\nu_r$ have again been observed for these process.[47] In many instances the RIACT approach performs a better conversion than its CW counterpart, opening the possibility of using mixed short-pulse/RIACT sequences that become less sensitive to the strength of quadrupolar couplings and therefore more quantitative than either option in Figure 9(a,b). Yet the actual fate of the spin-locked states will also depend on a competition between the strengths of the first order quadrupole coupling separating central from satellite transitions, the rf field recoupling these transitions, the spinning rate controlling the time that central and satellite transitions will stay in contact during the zero-crossings, and the various offsets involved. It is in fact illustrative to compare the predictions that the echo efficiency parameter ε introduced earlier yields for the two kinds of pulse sequences. For a typical case $S = 3/2$, the overall magnitudes of these coefficients are indeed larger for an optimized RIACT than for the short CW pulse sequence (Figure 11), yet the fact that they are also further spread out in their ϕ powder values is indicative of larger line shape distortions[54] and may prevent RIACT from achieving a more effective refocusing performance.

In addition to these sequences based on the implementation of $MQ \rightarrow 1Q$ conversions via the use of square CW rf pulses, a series of recent papers has focused on the application of shaped and variable-frequency pulses to MQMAS. A promising shaped-pulse proposition involves replacing the square conversion pulses by amplitude modulated ones.[38,39,42,45] This can be achieved via an actual modulation of the pulses' envelop, or by applying fast 180° phase shifts to the rf that will effectively split the on-resonance pulse into symmetric off-resonance components. Either approach can be used to efficiently excite the outlying satellite transitions involved in the 3Q → 1Q conversion step (Figure 9c). In spin-3/2 MQMAS experiments of simple model compounds, enhancement of over

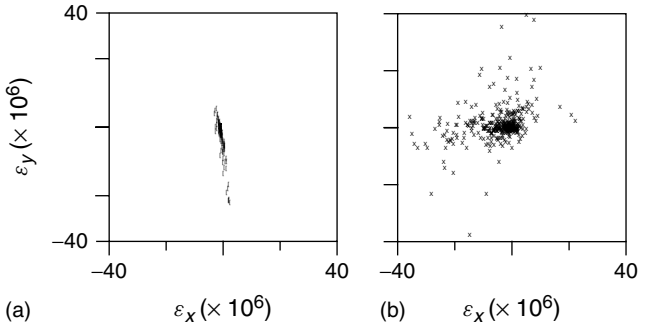

Figure 11 Comparison between the powder values taken by the $\{\varepsilon_\alpha\}_{\alpha=x,y}$ values in short-pulse (a) and RIACT MQMAS pulse sequences (b). Each point represents a different crystallite in the sample distributed over a solid sphere; both plots were calculated for identical MAS conditions: $S = 3/2$, $\nu_r = 10\,\text{kHz}$, $C_Q = \text{kHz}$, $\nu_1 = 100\,\text{kHz}$. Notice the overall larger magnitudes but also the spread of coefficients in the RIACT case (courtesy of A. Goldbourt and S. Vega, Weizmann Institute)

300% have recently been reported with this simple procedure. A closely related approach involves using double-frequency-swept chirp pulses, capable of enhancing the MQ conversion steps by sweeping through the off-resonance satellite transitions.[36,43] Theory predicts that either of these approaches may not perform as well for $S \geq 5/2$ spin systems as for their $S = 3/2$ counterparts. Still it has been shown that improvements can be achieved in some of these cases using pulses possessing a different amplitude modulation;[41,46] these approaches also appear promising for manipulating higher orders of MQ coherences.

Additional ways to improve the line shape and signal-to-noise in half-integer quadrupolar NMR in general have also been proposed; these are worth considering when implementing a low sensitivity experiment such as MQMAS. One of them takes advantage of the inhomogeneous nature of the anisotropies in MQMAS' direct dimension, to generate multiple 1Q signals from a single scan using a Carr–Purcell–Meiboom–Gill echo train during the acquisition period (Figure 9f).[44] Another involves transferring spin order from the satellite to the central spin transitions of a $S = 3/2$ prior to the beginning of the experiment, an approach that proves helpful when starting the spin excitation directly from central S_z^{2-3} magnetization as in the RIACT case.[48,55]

Most of these developments in pulse sequence focused on optimizing the MQMAS signal intensities in the presence of small off-resonance irradiation offsets. This is usually a very good approximation if alkali metals or light main group elements, possessing relatively small shielding contributions ($\leq 0.1\nu_1$). But for the case of heavier elements possessing much large magnitudes in their chemical shift scales, these offsets may severely interfere with the excitation of the MQ coherences. In some situations extreme shielding effects may prevent the acquisition of MQMAS signals altogether, even when dealing with sites possessing small quadrupole couplings. The effects of chemical shielding offsets can be compensated in part by manipulating the MQ coherences via the use of amplitude-modulated or composite pulses.[33] Still, even under these optimal conditions the overall MQMAS signal is usually poorer than that observed in the absence of large chemical or second order quadrupolar shifts.

Although more complete discussions on the optimization of these various MQMAS sequences can be found in the cited literature, it should be remembered that usually 'optimal' pulse values are just good initial starting points, susceptible to considerable improvement by even small variations in their timings. Before setting up a complete 2D MQMAS NMR acquisition it is therefore convenient to monitor the t_2 echo formation for a particular t_1 value, usually fixed at a small integer multiple of rotor periods in order to avoid the intense rotor-modulation imposed by spinning on MQMAS signals, and then vary the individual pulse width parameters around the suggested values until the strongest MQ signal has been detected. Only with these optimized values is it worth devoting the amount of spectrometer time that is required for the acquisition of a complete 2D MQMAS NMR spectrum.

4 FINE STRUCTURE OF THE MQMAS NMR LINE SHAPES

In addition to a successful refocusing of the interactions, retrieving quality half-integer quadrupolar line shapes by MQMAS demands dealing with a number of peculiarities related to the nature of this experiment. Most important among these is the presence of mixed-phase peak distortions. Mixed phase line shapes comprise one of the well-known limitations of 2D Fourier transform NMR, stemming from the indirect detection of one (or more) of the evolving frequencies.[20] Avoiding the dispersive artifacts that arise in these peaks requires some form of time-reversal involving either the formation of a spin-echo, the acquisition of separate echo/anti-echo or cosine/sine MQ-modulated signals (corresponding to different combinations of $+t_1$ and $-t_1$ evolutions), or the simultaneous acquisition of echo + anti-echo amplitude-modulated signals followed by their disentanglement via techniques such as time-proportional phase incrementation (TPPI) or off-resonance irradiation (discouraged for this experiment due to the reasons mentioned in the previous paragraph). Since MQMAS is actually an echo experiment, these mixed phase artifacts are not usually too severe. But when requiring highly-resolved or purely absorptive line shapes, the acquisition of echo and anti-echo signals with identical intensities for all crystallites is required. As mentioned earlier such acquisitions are in many instances hard or impossible to implement due to the different phase factors adopted by the ε parameter of the crystallites as a function of their orientation. Similar problems have been encountered in solution phase NMR, where it was shown they can be alleviated by introducing an intermediate step where coherences are momentarily stored along the z-axis and only then made into observable 1Q magnetizations. The resulting so-called z-filter approach (Figure 9d) ends up using a $0 \rightarrow \pm MQ(t_1) \rightarrow 0 \rightarrow -1(t_2)$ coherence transfer scheme, thereby requiring the addition of an extra pulse into the MQMAS sequence and sacrificing part of the signal.[24] On the other hand, the advantage of this z-filter lies in the fact that since efficiencies for $+MQ(t_1) \rightarrow 0 \rightarrow -1(t_2)$ and $-MQ(t_1) \rightarrow 0 \rightarrow -1(t_2)$ can now be made equal, purely absorptive 2D peaks result. Alternatively, mixed t_1 periods including both MQ and 1Q evolutions followed by acquisition of whole echoes over t_2 (Figure 9e,f) can be used to retrieve purely absorptive line shapes.[29,56] Further details on the nature of these distortions and on strategies for avoiding them are given in detail in (see **Advances in MQMAS NMR**).

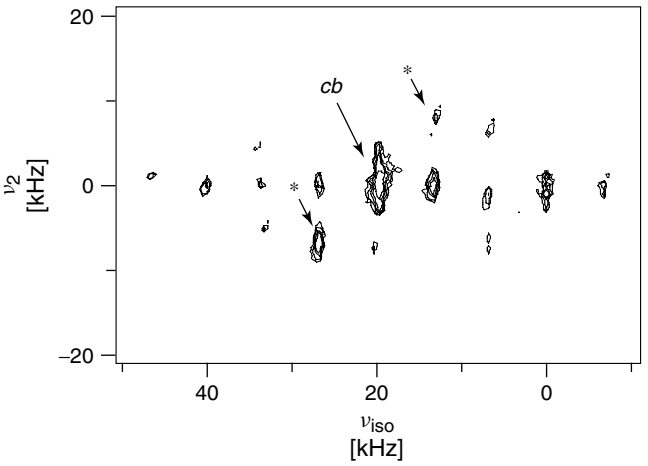

Figure 12 Spinning sideband structure displayed by the ^{23}Na MQMAS NMR spectrum of Na_2SO_4 recorded at 4.7 T with sample spinning at $\nu_r = 6$ kHz. Data were acquired using a two-pulse sequence (Figure 9a) and subject to a shearing to yield a high resolution dimension; they should lead to a single centerband (cb) peak. Asterisks indicate spinning sidebands originating from modulations of the central transition anisotropies, shifted along ν_1 as a result of a shearing of the data. All remaining spinning sidebands, appearing mainly along the indirectly detected ν_1 axis, are artifacts peculiar to the excitation and conversion orientation dependencies of the MQMAS pulse sequence (adapted from Ref.[57])

Another line shape feature characterizing MQMAS NMR spectra is the occurrence of extensive spinning sidebands in the indirectly detected MQ frequency domain (Figure 12). These sidebands behave like their conventional spin-1/2 counterparts in that they are absorptive and appear at multiples of the rotor frequency with decreasing intensities as the spinning speed is increased; their origin, however, does not necessarily relate to the usual spinning-induced time modulation of chemical shift, dipolar or second order quadrupolar interactions. Indeed MQMAS spinning sidebands can span a significantly larger frequency range than those corresponding to the static magnitudes of these nuclear interactions, and are often a consequence of the orientation dependencies associated with the nutation pulses used for MQ excitation and MQ detection.[57,58] A rigorous analysis of such problems requires introducing into the effects of the rf pulse involved in the MQMAS sequence, the explicit time-dependent oscillations of the first order quadrupolar frequencies during t_1. Such an approach reveals that the rotational sideband intensities are mainly a function of e^2qQ/h and η_Q; since analyses of the MQMAS frequency line shape can yield these internal coupling parameters, simulating these indirect-domain spinning sideband patterns often yields only redundant information. From this theoretical analysis it also follows that either orientation-independent excitation or conversion processes will be needed to remove the appearance of these artifacts; these goals have hitherto proved elusive to achieve.

Another source of MQMAS line shape distortions worth discussing are the nonsecular dipolar couplings that arise from other proximate quadrupole nuclei I. Such couplings have been extensively documented in ^{13}C MAS NMR, and are known to arise due to the quadrupole-induced tilting of I's

nuclear spin quantization axes.[59] These effects also show up in MQMAS NMR,[60–63] as neither the spin nor the spatial manipulations involved in this experiment can take care of their averaging. Such residual couplings can be of either homo- or heteronuclear nature, and their effects are usually smaller as magnetic fields increase. Of the various coupling scenarios, the simplest to describe is the high field heteronuclear one;[62] MQMAS line shapes here are made up of $2I + 1$ components whose centers of mass are placed at offsets

$$\nu_{\rm iso}(m_I) = \frac{[|C_S^4(m)| + 2mC_S^4\left(\frac{1}{2}\right)]}{C_S^4\left(\frac{1}{2}\right) + |C_S^4(m)|} \times \{[3m_I^2 - I(I+1)]\Delta + m_I J\} \qquad (15a)$$

where

$$\Delta = \frac{3}{20}\frac{D_{zz}^{\rm eff} C_Q^I}{\nu_O^I}(3\cos^2 b - 1 + \eta_Q^I \sin^2 b \cos 2a) \qquad (15b)$$

is a parameter depending on I's quadrupolar and Larmor as well as on I–S's dipolar coupling. As can be gathered from these expressions, such couplings are usually magnified by the MQMAS experiments, leading to complex multiplets that may impair the method's resolution (Figure 13) but which can also convey valuable coupling information.

Before concluding, it is worth dwelling on other issues affecting line shape resolution. When dealing with heteronuclear couplings to abundant spin-1/2 nuclei, such as in organic systems, the highest resolution proves hard to achieve by simple MAS averaging. This can be aided via heteronuclear decoupling, yet the magnification brought about by dealing with MQ evolutions may demand in these cases the use of efficient decoupling schemes for maximizing resolution.[64,65] Considerable resolution limitations can also arise in homonuclear systems from a different source: the flip-flop terms present in such dipole–dipole couplings, which do not commute with the longitudinal terms in the quadrupolar Hamiltonians.[74,78] If such homonuclear effects are present and strong, a fast-decaying MQMAS echo showing little resolution enhancement when compared to conventional MAS line shapes may result. Furthermore these effects may result in broadenings which decay only slowly or sometimes even increase with spinning speeds, at least within the range of normally used ν_r values.[66] Finally, it is also worth noting that a dependence of the spectral resolution has also been noted on the order m used in MQMAS experiments:[30,67,68] for $S \geq 5/2$ nuclei, a higher resolution tends to be achieved for the maximum MQ order available in the manifold. This can be rationalized by the different m-dependencies exhibited by the isotropic chemical and quadrupolar shifts, transforming as $2m$ and $C_O^S(m)$, respectively. The largest values of these weighting coefficients are usually found for the $m_1 = S$ condition; a $-S \rightarrow -1$ coherence transfer pathway is then required for achieving a refocusing of anisotropies and this choice further reinforces the resolving power of the various isotropic contributions along the high resolution domain. Even further refinements on this approach can be proposed if one allows the pulse sequence to subsequently encode several MQ orders throughout the course of the indirect t_1 evolution;[69] it then becomes feasible to devise acquisition schemes that maximize resolution for almost arbitrary shift values, even if at the expense of substantial sacrifices in signal-to-noise.

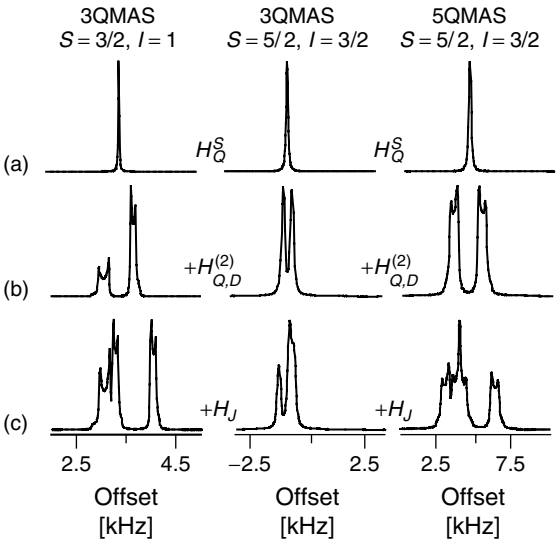

Figure 13 Progressive broadening introduced into the isotropic dimension of MQMAS line shapes (a) by the residual dipolar (b) and J (c) couplings between a spin S and a quadrupolar heteronucleus. Tensors were in all cases assumed axially symmetric and coincident, and the frequency scales refer to an isotropic shift $\delta_S = 0$ kHz. Spectra on the left assumed 3QMAS NMR on an $S = 3/2$ ($e^2qQ/h = 2$ MHz, $\nu_O = 64.4$ MHz) coupled to an $I = 1$ ($e^2qQ/h = 3$ MHz, $\nu_O = 14.5$ MHz) with a $D_{zz}^{\rm eff} = 1.7$ kHz; the center and right columns describe the 3QMAS and 5QMAS spectra of an $S = 5/2$ ($e^2qQ/h = 3$ MHz, $\nu_O = 52$ MHz) coupled to an $I = 3/2 (e^2qQ/h = 12$ MHz, $\nu_O = 20$ MHz). J couplings throughout row (c) were set at 100 Hz (adapted from Ref.[62])

5 OUTLOOK

This review discussed some of the basic features of 2D MQMAS NMR as they apply to the acquisition of high resolution spectra from half-integer quadrupolar nuclei. As an analytical tool for resolving inequivalent chemical sites, the technique appears to be experimentally simple and applicable to a large number of elements. It can be used to distinguish isotropic chemical from isotropic quadrupolar shifts, as well as to pinpoint the quadrupolar coupling parameters e^2Qq/h and η_Q of individual chemical sites. Remarkable also is the extensive spin-physics that have been triggered by this experiment, reawakening a mostly dormant interest in the field of MQ quadrupolar NMR in solids. Due to space constraints many of the underlying principles developed in connection with the manipulation of MQ coherences throughout this experiment have only been briefly discussed. As mentioned, this material is covered in further detail in the original literature, in a number of recent reviews[70–73] as well as in accompanying articles in this Encyclopedia.

As the number of MQMAS applications continues to grow, a number of challenges to be resolved are also becoming increasingly clear. Some of these are of a technical nature, and involve issues such as employing MQMAS data for quantifying the abundance of chemical sites and/or for improving the signal-to-noise ratio of the experiment. Indeed, although significant advances have been made in these areas important

obstacles to overcome still remain, for instance when it comes to observing low-γ nuclei, to characterizing systems affected by substantial chemical shieldings, or to unlocking the potential of 5Q and 7Q MAS spectroscopies towards improving the spectral resolution. Yet it is also clear that even in its present form MQMAS can be a significant aid in enhancing the NMR information afforded by a variety of chemical systems.

A second and perhaps longer-range type of problem triggered by MQMAS, stems from the nature of the method as a mean rather than as an end. Indeed, once inequivalent resonances appear resolved by MQMAS, the real problem of analyzing the meaning of these NMR data begins. For many of the spin isotopes being analyzed by MQMAS this challenge is currently hard to overcome, as the assignment of quadrupolar and shielding parameters to individual chemical sites remains for the most part uncharted. Quantum chemical calculations of NMR coupling parameters are a potentially good starting point for establishing such correlations, yet in many instances their usefulness is compromised by the heavy-element and multi-electronic nature of the isotopes being analyzed. An alternative to this assignment approach relies on employing the X-ray structures available for model systems, in combination with spectral editing techniques based on the dipolar dephasing imposed by nearby nuclei, in order to empirically correlate MQMAS-resolved coupling parameters with specific coordination and bonding motifs. This in turn highlights the need to further develop homo- and heteronuclear recoupling techniques on quadrupole nuclei, and for making these recoupling protocols integral parts of the MQMAS methodology. Driven by this need, it is reasonable to expect this research area to become within the near future as active a topic of investigation as it has become for its spin-1/2 counterparts.

6 RELATED ARTICLES IN THIS VOLUME

Advances in MQMAS NMR; Satellite Transition NMR Spectroscopy of Half-Integer Quadrupolar Nuclei under Magic-Angle Spinning.

7 RELATED ARTICLES IN VOLUMES 1–8

Dynamic Angle Spinning, Volume 3; Magic Angle Spinning, Volume 5; Multidimensional Spectroscopy: Concepts, Volume 5; Multiple Quantum Spectroscopy of Liquid Samples, Volume 5; Quadrupolar Interactions, Volume 6; Quadrupolar Nuclei in Solids, Volume 6.

8 REFERENCES

1. R. K. Harris and B. E. Mann, 'NMR and the Periodic Table', Academic Press: New York, 1970.
2. M. H. Cohen and F. Reif, *Solid State Phys.*, 1957, **5**, 321–438.
3. C. P. Slichter, 'Principles of Nuclear Magnetic Resonance', 3rd edn., Springer-Verlag: New York, 1990.
4. D. Freude and J. Haase, *NMR Basic Principles Prog.*, 1993, **29**, 1–90.
5. B. F. Chmelka and J. W. Zwanziger, *NMR Basic Principles Prog.*, 1994, **33**, 79–123.
6. A. J. Vega, in 'Encyclopedia of NMR', eds D. M. Grant and R. K. Harris, Wiley: New York, 1996, pp 3869–3888.
7. M. M. Maricq and J. S. Waugh, *J. Chem. Phys.*, 1979, **70**, 3300–3316.
8. G. E. Maciel, *Science*, 1984, **226**, 282–288.
9. E. Oldfield and R. J. Kirkpatrick, *Science*, 1985, **227**, 1537–1544.
10. J. Fitzgerald, 'Solid State NMR of Inorganic Materials', ACS Symposium Series No. 717, ACS: Washington, DC, 1999.
11. A. Llor and J. Virlet, *Chem. Phys. Lett.*, 1988, **152**, 248–253.
12. A. Samoson, A. Lippmaa, and A. Pines, *Mol. Phys.*, 1988, **65**, 1013–1016.
13. K. T. Mueller, B. Q. Sun, G. C. Chingas, J. W. Zwanziger, T. Terao, and A. Pines, *J. Magn. Reson.*, 1990, **86**, 470–487.
14. L. Frydman and J. S. Harwood, *J. Am. Chem. Soc.*, 1995, **117**, 5367–5368.
15. A. Medek, J. S. Harwood, and L. Frydman, *J. Am. Chem. Soc.*, 1995, **117**, 12 779–12 787.
16. U. Haeberlen, in 'Advances in Magnetic Resonance', ed J. S. Waugh, Academic Press: New York, 1976.
17. L. Frydman, *Ann. Rev. Phys. Chem.*, 2001, **52**, 463–498.
18. E. R. Andrew, A. Bradbury, and R. G. Eades, *Nature*, 1958, **182**, 1659–1659.
19. E. W. Wooten, K. T. Muller, and A. Pines, *Acc. Chem. Res.*, 1992, **25**, 209–215.
20. R. R. Ernst, G. Bodenhausen, and A. Wokaun, 'Principles of Nuclear Magnetic Resonance in One and Two Dimensions', Clarendon: Oxford, 1987.
21. S. P. Brown, S. J. Heyes, and S. Wimperis, *J. Magn. Reson.*, 1996, **A119**, 280.
22. Z. H. Gan, *J. Am. Chem. Soc.*, 2000, **122**, 3242–3243.
23. J. P. Amoureux, C. Fernandez, and L. Frydman, *Chem. Phys. Lett.*, 1996, **259**, 347–355.
24. J. P. Amoureux, C. Fernandez, and S. Steuernagel, *J. Magn. Reson.*, 1996, **A123**, 116–118.
25. D. Massiot, *J. Magn. Reson.*, 1996, **A122**, 240–244.
26. G. Wu, D. Rovnyak, and R. G. Griffin, *J. Am. Chem. Soc.*, 1996, **118**, 9326–9332.
27. G. Wu, D. Rovnyak, B. Sun, and R. G. Griffin, *Chem. Phys. Lett.*, 1996, **249**, 210–217.
28. J. P. Amoureux and C. Fernandez, *Solid State NMR*, 1996, **5**, 315–321.
29. S. P. Brown and S. Wimperis, *J. Magn. Reson.*, 1997, **128**, 42–61.
30. M. J. Duer and C. Stourton, *J. Magn. Reson.*, 1997, **124**, 189–199.
31. M. Hanaya and R. K. Harris, *J. Phys. Chem.*, 1997, **A101**, 6903–6910.
32. F. H. Larsen, H. J. Jakobsen, P. D. Ellis, and N. C. Nielsen, *J. Phys. Chem. A*, 1997, **101**, 8597–8606.
33. L. Marinelli, A. Medek, and L. Frydman, *J. Magn. Reson.*, 1998, **132**, 88–95.
34. J. P. Amoureux, M. Pruski, D. P. Lang, and C. Fernandez, *J. Magn. Reson.*, 1998, **131**, 170–175.
35. S. Ding and C. A. McDowell, *J. Magn. Reson.*, 1998, **135**, 61.
36. A. P. M. Kentgens and R. Verhagen, *Chem. Phys. Lett.*, 1999, **300**, 435–443.
37. F. H. Larsen and N. Nielsen, *J. Phys. Chem. A*, 1999, **103**, 10 825–10 832.
38. P. K. Madhu, A. Goldbourt, L. Frydman, and S. Vega, *Chem. Phys. Lett.*, 1999, **307**, 41–47.
39. P. K. Madhu, A. Goldbourt, L. Frydman, and S. Vega, *J. Chem. Phys.*, 2000, **112**, 2377.
40. J. P. Amoureux, J. W. Wiench, and M. Pruski, *J. Magn. Reson.*, 2000, **147**, 286–295.
41. A. Goldbourt, P. K. Madhu, and S. Vega, *Chem. Phys. Lett.*, 2000, **320**, 448–456.
42. A. Goldbourt, P. K. Madhu, S. Kababya, and S. Vega, *Solid State NMR*, 2000, **18**, 1–16.
43. D. Iuga, H. Schafer, R. Verhagen, and A. P. M. Kentgens, *J. Magn. Reson.*, 2000, **147**, 192–209.

44. T. Vosegaard, F. H. Larsen, H. J. Jakobsen, P. D. Ellis, and N. C. Nielsen, *J. Am. Chem. Soc.*, 1997, **11**, 9055.
45. T. Vosegaard, P. Florian, P. J. Grandinetti, and D. Massiot, *J. Magn. Reson.*, 2000, **143**, 217–222.
46. T. Vosegaard, D. Massiot, and P. J. Grandinetti, *Chem. Phys. Lett.*, 2000, **326**, 454–460.
47. T. Vosegaard, P. Florian, D. Massiot, and P. J. Grandinetti, *J. Chem. Phys.*, 2001, **114**, 4618.
48. H.-T. Kwak, S. Prassad, Z. Yao, L. Emsley, J. Sachleben, and P. J. Grandinetti, *J. Magn. Reson.*, 2001, **150**, 71–80.
49. A. Wokaun and R. R. Ernst, *J. Chem. Phys.*, 1977, **67**, 1752–1758.
50. S. Vega, *J. Chem. Phys.*, 1978, **68**, 5518.
51. S. Vega and Y. J. Naor, *J. Chem. Phys.*, 1981, **75**, 75–86.
52. R. Jannsen and W. S. Veeman, *J. Chem. Soc., Faraday Trans.*, 1988, **84**, 3747.
53. A. J. Vega, *J. Magn. Reson.*, 1992, **96**, 50–68.
54. K. H. Lim and C. P. Grey, *Solid State NMR*, 1998, **13**, 101.
55. Z. Yao, H.-T. Kwak, D. Sakellariou, L. Emsley, and P. J. Grandinetti, *Chem. Phys. Lett.*, 2000, **327**, 85–90.
56. D. Massiot, B. Tonzo, D. Trumeau, J. P. Coutures, J. Virlet, P. Florian, and P. J. Grandinetti, *Solid State NMR*, 1996, **6**, 73–83.
57. L. Marinelli and L. Frydman, *Chem. Phys. Lett.*, 1997, **275**, 188–198.
58. U. Friedrich, I. Schnell, S. P. Brown, A. Lupescu, D. E. Demco, and H. W. Spiess, *Mol. Phys.*, 1998, **95**, 1209–1227.
59. R. K. Harris and A. C. Olivieri, *Prog. NMR Spetrosc.*, 1992, **24**, 435–456.
60. J. McManus, R. Kemp-Harper, and S. Wimperis, *Chem. Phys. Lett.*, 1999, **311**, 292–298.
61. G. Wu and K. Yamada, *Chem. Phys. Lett.*, 1999, **313**, 519–524.
62. S. Wi and L. Frydman, *J. Chem. Phys.*, 2000, **112**, 3248–3261.
63. S. Wi, V. Frydman, and L. Frydman, *J. Chem. Phys.*, 2001, **114**, 8511–8519.
64. V. Lacassagne, P. Florian, V. C. Montouillout, F. B. Gervais, and D. Massiot, *Magn. Reson. Chem.*, 1998, **36**, 956.
65. A. E. Bennett, C. M. Rienstra, M. Auger, K. V. Lakshmi, and R. G. Griffin, *J. Chem. Phys.*, 1995, **103**, 6951–6958.
66. M. Eden and L. Frydman, *J. Chem. Phys.*, 2001, **114**, 4116–4123.
67. S. H. Wang, Z. Xu, J. H. Baltisberger, L. M. Bull, J. F. Stebbins, and A. Pines, *Solid State NMR*, 1997, **8**, 1–16.
68. K. J. Pike, R. P. Malde, S. E. Ashbrook, J. McManus, and S. Wimperis, *Solid State NMR*, 2000, **16**, 203.
69. A. Jerschow, J. W. Logan, and A. Pines, *J. Magn. Reson.*, 2001, **149**, 268–270.
70. A. Medek and L. Frydman, *J. Braz. Chem. Soc.*, 1999, **10**, 263–277.
71. D. Freude, in 'Encyclopedia of Analytical Chemistry', ed R. A. Meyers, Wiley: Chichester, 2000, pp 12 188–12 224.
72. M. E. Smith and E. R. H. vanEck, *Prog. NMR Spectrosc.*, 1999, **34**, 159–201.
73. M. W. Anderson and M. J. Duer eds, New NMR Techniques for Quadrupolar Nuclei, in *Solid State NMR*, 1999, **15**.
74. C. V. Grant, D. McElheny, V. Frydman, and L. Frydman, manuscript in preparation.
75. H. Kessler, M. Gehrke, and C. Griesinger, *Angew. Chem. Int. Ed. Engl.*, 1988, **27**, 490–536.
76. C. A. Fyfe, J. Skibsted, H. Grodney, and H. M. Altenschildesche, *Chem. Phys. Lett.*, 1997, **281**, 44–48.
77. M. J. Duer, *Chem. Phys. Lett.*, 1997, **277**, 167–174.
78. M. J. Duer and A. J. Painter, *Chem. Phys. Lett.*, 1999, **313**, 763–770.

Acknowledgements

The development of the material described in this paper was enriched by valuable discussions with Dr Ales Medek, Ms Laura Marinelli, Dr John S. Harwood, Dr Chris Grant, Dr P. K. Madhu and Professor S. Vega.

Biographical Sketch

Lucio Frydman, *b* 1965, Buenos Aires, Argentina. B.Sc. 1986 Chemistry, Ph.D. 1990 Physical Chemistry, University of Buenos Aires. Research Associate, Lawrence Berkeley Laboratory, 1990–1992 with A. Pines. Assistant-Associate-Full Professor, University of Illinois at Chicago, 1992–2001. Adjunct Professor, University of Illinois at Chicago, since 2001. Professor, Weizmann Institute of Sciences, since 2001. Approximately 70 publications. Current research interests: development and application of new methods in solution solid state and liquid crystalline NMR.